PCCP

PAPER

View Article Online
View Journal | View Issue

Hydrogen defects in tetragonal ZrO_2 studied using density functional theory†

Cite this: *Phys. Chem. Chem. Phys.*, 2014, **16**, 1354

Mostafa Youssef and Bilge Yildiz*

In the energy-structure paradigm, we analyzed the defects that can arise in tetragonal zirconium oxide (T-ZrO_2) involving the hydrogen atom or the hydrogen molecule using density functional theory. Our results indicate that the dominant hydrogen defect under reducing conditions is $H_O^{\bullet}$, a complex formed between the hydride ion and a doubly charged oxygen vacancy. This result is consistent with the experimental observation that under reducing conditions, the solubility of hydrogen is proportional to the degree of hypostoichiometry of T-ZrO_2. Under oxidizing conditions we found three different hydrogen defects, each predominating in a specific range of the chemical potential of electrons. Starting from the valence band top toward the conduction band bottom, these defects are the interstitial proton, $H_i^{\bullet}$, a complex formed between two hydrogen species and a zirconium vacancy with a net effective charge of (2−), $(2H)_{Zr}''$, and finally a complex similar to the latter but with a net effective charge of (4−), $(H_2)_{Zr}''''$. In $(2H)_{Zr}''$ the two hydrogens exist in the form of hydroxyl groups, while in $(H_2)_{Zr}''''$ they exist in the form of a hydrogen molecule. In addition, we found that up to three hydrogen species can favorably accumulate in a zirconium vacancy under oxidizing conditions. The clustering of hydrogen in cation vacancies can be a precursor for the deleterious effects of hydrogen on the mechanical properties and stability of metal oxides, in analogy with hydrogen embrittlement in metals. Finally we observed a red-shift and a blue-shift for the vibrational frequencies of all the hydroxyl groups and all the hydrogen molecules, respectively, in T-ZrO_2 when compared to the gas phase frequencies. This is an important characteristic for guiding future experimental efforts to detect and identify hydrogen defects in T-ZrO_2. The insights presented in this work advance our predictive understanding of the degradation behavior of T-ZrO_2 as a corrosion resistant passive layer, as a gate dielectric and in biomedical applications.

Received 1st October 2013,
Accepted 11th November 2013

DOI: 10.1039/c3cp54153c

www.rsc.org/pccp

1. Introduction

The hydrogen atom (H), the di-hydrogen cation (H_2^+), and the heavy hydrogen nucleus (^2H) are the simplest model systems and standard textbook examples in quantum mechanics, molecular orbital theory, and nuclear physics, respectively. In spite of this apparent simplicity of hydrogen, its interactions in condensed matter are nontrivial and lead to a variety of complex phenomena such as hydrogen embrittlement,[1] hydrogen multicenter bonds,[2] and the elusive hydrogen bond[3] to name but a few.

A condensed matter system of utmost technological importance is zirconium oxide (ZrO_2). Zirconia's applications include protection against corrosion of nuclear fuel rods,[4] fuel cell electrolytes,[5] gate dielectric for metal oxide semiconductor devices,[6] and hip implants.[7] The tetragonal phase of zirconia (T-ZrO_2) stands out as the corrosion resistant,[4] mechanically the toughest,[8,9] and the one with the highest dielectric constant among the three low-pressure polymorphs of zirconia (monoclinic, tetragonal, and cubic).

The goal of this paper is to unravel the complex interaction between hydrogen and tetragonal zirconium oxide. In particular we used density functional theory to study the energy and structure of hydrogen point defects and defect complexes that can arise in T-ZrO_2. The urge to thoroughly understand the physics of hydrogen defects in T-ZrO_2 arises in different fields. We briefly describe here three examples.

In light water nuclear reactors zirconium alloys are used as cladding for the nuclear fuel. Zirconia passive layers grow on the cladding alloy due to the corrosion of zirconium in high temperature water.[10] Hydrogen is a byproduct of the corrosion reaction and a fraction of it penetrates the zirconium oxide layers until it reaches the zirconium metal and eventually hydrogen degrades the metal in a process known as hydrogen embrittlement.[11] Since zirconia, and especially the tetragonal

Laboratory for Electrochemical Interfaces, Department of Nuclear Science and Engineering, Massachusetts Institute of Technology, 77 Massachusetts Avenue, Cambridge, Massachusetts 02139, USA. E-mail: byildiz@mit.edu

† Electronic supplementary information (ESI) available. See DOI: 10.1039/c3cp54153c

phase that is interfacing with the metal,[4] is the route for hydrogen to reach the underlying metal, it is necessary to understand the form in which hydrogen can exist in T-ZrO_2. This knowledge can then be used for assessing the mobility of the relevant hydrogen defects and ultimately their diffusion kinetics towards the metal/oxide interface.

Zirconia was suggested to replace silica in metal oxide semiconductor devices due to its good thermal stability and high dielectric constant.[6] However, hydrogen is unintentionally incorporated in ZrO_2 films during the manufacturing process. Some of the incorporated hydrogen persists in the oxide in spite of post annealing. The adverse consequence is that certain forms of hydrogen defects can lead to undesirable fixed charge in the oxide[12] and can further reduce its dielectric constant.[13] Thus, mitigating these adverse effects of hydrogen requires a fundamental understanding of how it exists in zirconia films which can contain the tetragonal phase after the annealing process.[6]

Our final example comes from the biomedical applications of zirconia as in hip implants and dental restorations. These applications of zirconia rely on stabilizing the tetragonal phase since it exhibits high fracture toughness. However, the continuous exposure of T-ZrO_2 to moisture in a range of temperatures (30–300 °C) leads eventually to an expansive phase transformation to the monoclinic phase. The volume expansion accompanying this phase transformation leads to severe degradation and cracking of the oxide and hence limits its long term stability during usage. This phenomenon is known as the low temperature degradation of T-ZrO_2.[8,9] All the attempts to explain and overcome this phenomenon relate to hydrogen defects that appear in T-ZrO_2 as a consequence of water splitting on the surface of the oxide.[8,9]

Although the above examples clearly point toward the need for a thorough and a fundamental understanding of hydrogen defects in tetragonal ZrO_2, up until now this has not been realized. The earliest attempts to elucidate the types of hydrogen defects in zirconia and particularly the tetragonal phase were motivated by the nuclear industry as described in the first example above and relied on the measurement of hydrogen permeability and solubility in zirconia.[14,15] Collectively these experiments suggested that, under reducing conditions, oxygen vacancies are needed for the dissolution and migration of hydrogen in ZrO_2. More recently, muon spin spectroscopy experiments[16] were performed on wide band gap oxides and focused on identifying the charge state of interstitial hydrogen (indeed the analysis did not account for any possibility of hydrogen trapping in the native defects). The results suggested that in monoclinic ZrO_2 neutral interstitial hydrogen, $H_i^{\times}$, predominates at low temperatures (10–100 K) while at higher temperatures (300–600 K) a diamagnetic form of hydrogen, $H_i^{\bullet}$ or H_i', predominates.

Atomistic simulations using density functional theory (DFT) were proved to be a powerful tool in studying hydrogen defects in metals,[17–20] and semiconductors and insulators.[2,21–29] In spite of this, only very few studies have appeared recently to address specific types of hydrogen defects in monoclinic[21,22] and yttria stabilized cubic zirconia.[30] For tetragonal zirconia, Shluger *et al.*, in their review article about atomisitc simulation of defects in wide band gap oxides,[6] considered performing a brief DFT comparison between the interstitial proton and the interstitial neutral hydrogen atom. They showed that the interstitial proton is stable and binds to one of the lattice oxygens to form a hydroxyl group, while the neutral interstitial hydrogen is only metastable and the electron delocalizes immediately leaving the interstitial proton behind upon thermal activation.

Given the importance of deciphering the nature of hydrogen defects in T-ZrO_2, and the current status of our limited knowledge about these defects, we performed a comprehensive DFT investigation of the energetics and structure of hydrogen defects and defect complexes in T-ZrO_2. We identified the hydrogen defects that predominate separately under oxygen rich and oxygen poor conditions. In addition, we introduced a thorough formulation for the binding energy of a defect complex with physical constraints, and with it, quantified the thermodynamic stability of the complexes that forms between the hydrogen and the native defects of T-ZrO_2. Finally, we examined the electronic and atomic structure of all hydrogen-related defects and computed the vibrational frequencies of the hydroxyl group or hydrogen molecule that may exist in these defects. The latter computation is useful in guiding future experimental efforts to detect and identify hydrogen defects in T-ZrO_2.

2. Theoretical and computational approaches

2.1 Defect structures and charges

We considered the defects that can arise in bulk tetragonal zirconia due to both hydrogen atom and hydrogen molecule. These defects can be classified according to the lattice site as an interstitial, a complex with an oxygen vacancy and a complex with a zirconium vacancy. The native interstitial defects were found to have very low concentrations[31] and hence their complexes with hydrogen were not considered here. We describe here the structures we investigated for these defects and the logic behind the charge states that we examined for each.

The initial guess for hydrogen complexes with native vacancies was obtained by replacing zirconium or oxygen with a hydrogen atom or molecule. In the case of the molecule, the center of the H_2 molecule was placed coincident with the site that was originally occupied by oxygen or zirconium. We considered 5 possible orientations of the H_2 molecule in 5 nonequivalent crystallographic directions which are ⟨001⟩, ⟨100⟩, ⟨110⟩, ⟨101⟩, and ⟨111⟩. In most cases after relaxation, the molecule splits into two hydrogen species, as will be presented in the Results and discussion section.

We performed an extensive search for the lowest energy interstitial site for the mono-hydrogen. We considered five dumbbell configurations (in some literature termed anti-bonding sites) formed by the lattice oxygen and the interstitial hydrogen in the crystallographic directions ⟨001⟩, ⟨100⟩, ⟨110⟩, ⟨101⟩, and ⟨111⟩, and two dumbbell configurations formed by the lattice zirconium and the interstitial hydrogen in ⟨001⟩ and ⟨100⟩. We also examined two so-called bond center sites by inserting the interstitial hydrogen

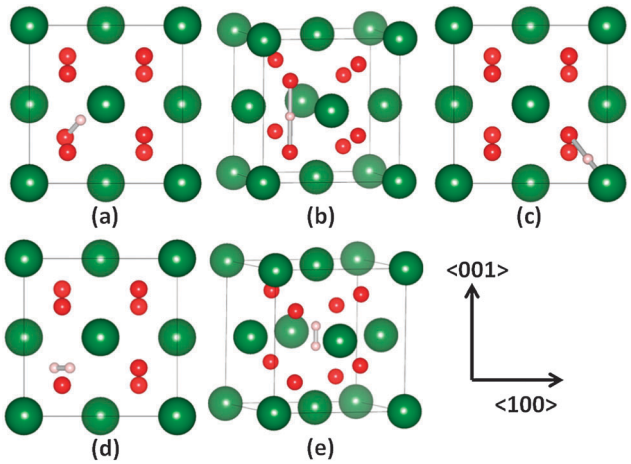

Fig. 1 Representative hydrogen defect structures. Interstitial mono-hydrogen: (a) forming a ⟨111⟩ dumbbell with lattice oxygen, (b) in a ⟨001⟩ crowdion site between two lattice oxygens, and (c) in a bond center site. Hydrogen molecule: (d) substituting a lattice oxygen and oriented in ⟨110⟩, and (e) in an interstitial octahedral site and oriented in ⟨001⟩. Green (large), red (medium), and white (small) balls represent zirconium, oxygen, and hydrogen, respectively. The sticks are guides for the eye and have no physical significance.

at the center of the bond between zirconium and oxygen. There are two distinct bond center sites because of the tetragonal distortion of the oxygen columns in tetragonal zirconia. Finally, we considered interstitial hydrogen in the octahedral site, *i.e.*, in the middle of the conventional unit cell of T-ZrO_2 and in two crowdion sites in the directions ⟨001⟩ and ⟨100⟩. The interstitial hydrogen molecule was examined by placing its center in the octahedral site and allowing it to take one of five orientations in the directions ⟨001⟩, ⟨100⟩, ⟨110⟩, ⟨101⟩ and ⟨111⟩. For illustration, we show in Fig. 1 representative examples of the defect structures that we summarized above.

For each one of the hydrogen defect configurations described above, we examined multiple possible charge states. The rationale behind what was considered as a possible charge state is the following. We regard the zirconium vacancy, oxygen vacancy, and both the atomic and molecular interstitial hydrogens as elementary defects. Each of these elementary defects, D, can have a charge state that ranges from q^{D}_{min} to q^{D}_{max}. The values of these two extrema were taken to be (4−,0), (0,2+), (−,+) and (−,+) for zirconium vacancy, oxygen vacancy, and atomic and molecular interstitial hydrogen, respectively. For both the cation and anion vacancies, a wider range of charge states is possible, however, modeling these extra charge states need computationally expensive non-local DFT functionals and they are anticipated to have high formation energies.[32–34] When a complex is formed as the union of two elementary defects (D_1,D_2), its charge state can in principle take any value in the range from $q^{D_1}_{min} + q^{D_2}_{min}$ to $q^{D_1}_{max} + q^{D_2}_{max}$. This simple rule sets the ground for a systematic way to investigate the possible charge states for charged defect complexes.

However, not every charge state expected for the defect complex based on the previous rule can be actually realized. As extensively discussed in ref. 35 and 36 certain charge states (including neutral) may not be possible to realize because the last added electron (hole) does not localize on the defect and favors relaxation into the conduction (valence) band. Examining the charge density and the net spin density, and performing Bader charge analysis[37,38] in addition to the criteria suggested in ref. 35 were our tools to investigate and decide charge localization on the defect. Kröger–Vink notation for charged defects will be used throughout the paper.

So far we have presented a systematic way to investigate the possible configurations and charge states of atomic and molecular hydrogen defects in T-ZrO_2. However, there is evidence both from our results discussed below and from prior DFT calculations[39] on Al_2O_3 that hydrogen can cluster in the cation vacancy. This phenomenon can have a significant deleterious impact on the mechanical stability of metal oxides as hydrogen is known to be a bond breaker.[26] As a technological consequence of this, the metal oxide can fail to act as a protective passive layer for the underlying metal in a corrosive environment. Thus, it is important to quantify the energetics and understand the structure of these clusters in order to assess any potential degradation of the mechanical properties of the metal oxide. However, once the number of hydrogen species in a defect exceeds two, the possible configurations and charge states become intractable. In spite of that our systematic investigation guided us to intuitively consider only two important clusters between hydrogen and zirconium vacancy. Those are $(3H)_{Zr}$ in the charge state (−) and $(4H)_{Zr}$ in the charge state (0). The rationale behind our choice of those two particular defects will be examined in detail in Section 3.2. Here we suffice to state that these combinations of the number of hydrogen species and the charge of the defect lead to hole-free oxygen ions around the defect which is energetically favorable.

2.2 Defect energetics

The abundance and stability of hydrogen defects were characterized by two energy metrics; the formation energy and the binding energy, respectively. While the former metric is applicable to any defect, the latter is devoted to complexes. The theoretical formalism to understand the energetics of defect equilibria is detailed elsewhere;[31,40] here we summarize the relevant notions.

The formation energy of a defect D with charge q is denoted by $E^{f}_{D,q}$ and defined as:

$$E^{f}_{D,q} = E_{defected} - E_{perfect} + \sum_{k} \Delta n_k \mu_k + q(E_{VBM} + \mu_F) + E_{MP}, \quad (1)$$

where $E_{defected}$ and $E_{perfect}$ are the DFT energies of the supercell that contains the defect and the perfect crystal supercell, respectively. Δn_k is the number of atoms of the species k in the perfect crystal supercell minus the number of the atoms of the same species in the defective cell. μ_k is the chemical potential of the species k, E_{VBM} is the energy of the valence band maximum in the perfect crystal supercell, and μ_F is the chemical potential of electrons (or the Fermi level) referenced to the valence band maximum of the prefect crystal. Thus, μ_F can take a value in the range from 0 to the value of the width of the band gap in the perfect crystal. The latter was found to be

3.9 eV in our earlier work.[31] Finally, E_{MP} is the Makov–Payne correction.[41] In applying this correction, we used the experimental value[42] for the static dielectric constant of yttria-stabilized tetragonal zirconia 39.8, which is in a good agreement with the DFT predicted value of 42 for undoped zirconia.[43] As demonstrated in our previous work on the native defects of tetragonal zirconia,[31] considering the leading term of this correction is adequate in comparison with the computationally expensive finite size scaling correction.[44] We demonstrate this adequacy also for selected hydrogen defects in the ESI.† In particular we found the absolute error in the formation energies to be within 0.3 eV from the values obtained by finite size scaling for hydrogen defects.

In thermodynamic equilibrium, there are constraints on the chemical potentials of the species present in T-ZrO_2. The chemical potential of oxygen, μ_O, in T-ZrO_2 cannot exceed the chemical potential of the oxygen atom in the O_2 molecule in the gas phase. The latter is taken as 1/2, the DFT energy of the oxygen molecule, thus, $\mu_O \leq \frac{1}{2}E^{DFT}_{O_2}$. The chemical potential of hydrogen is constrained in the same way and hence, $\mu_H \leq \frac{1}{2}E^{DFT}_{H_2}$. Similarly, the upper bound of the chemical potential of zirconium, μ_{Zr}, in T-ZrO_2 is the chemical potential of the zirconium atom in bulk zirconium metal. The latter is taken to be the DFT calculated cohesive energy of zirconium atom in hexagonal close-packed zirconium, thus, $\mu_{Zr} \leq E^{DFT}_{Zr\text{-metal}}$. The lower bounds of the chemical potentials of both zirconium and oxygen are constrained by the expression: $2\mu_O + \mu_{Zr} = E^{DFT}_{ZrO_2}$, where $E^{DFT}_{ZrO_2}$ is the DFT calculated energy of the ZrO_2 unit formula in the bulk of perfect crystal T-ZrO_2. Finally, the introduction of hydrogen into the system imposes an additional constraint, which is: $2\mu_H + \mu_O \leq E^{DFT}_{H_2O}$, where $E^{DFT}_{H_2O}$ is the DFT calculated energy of the water molecule in the gas phase. In our modeling for hydrogen defects in tetragonal zirconia, we considered the two extremes which are oxygen rich (zirconium poor) and oxygen poor (zirconium rich). The chemical potential of hydrogen was always set to the highest value possible (hydrogen rich) but limited by the formation of water as discussed above. The values of the chemical potentials of all the species in the two limiting cases and the DFT energies of the reference states that set the bounds discussed above are summarized in the ESI.†

The binding energy is a measure of the thermodynamic stability of a complex against dissociation into its constituents. We define the binding energy, E_b, of a complex C whose charge is q to be:

$$E_b = \max\left(E^f_{C,q} - \sum_k{}''' E^f_{D_k,q_k}\right), \quad (2)$$

where k represents each constituent defect of the complex C, and the triple prime over the summation sign indicates the three constraints imposed on the summation. The first is the conservation of species, that is the defects D_1, D_2, ... when combined together have to be chemically equivalent to the complex C. The second constraint is the conservation of charge, that is $q = \sum_k q_k$. *Thus, the binding energy is neither dependent on the chemical potential of species forming the complex, nor the chemical potential of electrons*. The third constraint is physically motivated, and discards the dissociation pathways for the complex that can lead to the formation of a disallowed charge state for certain constituent defects, D_k. The last constraint is concerned with the defects that exhibit negative-U behavior. The latter are the singly charged oxygen vacancy as shown in our previous study on the native defects,[31] and the neutral interstitial hydrogen atom as will be discussed in the Results and discussion section. The max function in the definition indicates that the stability of the complex is determined by its easiest dissociation pathway. This is an important point to emphasize as we believe that most of the binding energy values for hydrogen complexes in ionic materials reported in the literature are somewhat exaggerated because of limiting the search to only one dissociation pathway. To the best of our knowledge, only the work of Kang *et al.* on hydrogen defects in HfO_2 considered this important constraint.[12] A concrete example for the application of the above definition is discussed in detail in the ESI.† The convention we adopt for the binding energy in eqn (2) is such that negative values indicate stable complexes and positive values indicate unstable complexes.

Strictly speaking the binding energy alone is not enough to characterize the stability of defect complexes. A better metric would be, $-E_b + E_a$, where E_a is the activation energy needed for the dissociation of the constituents of the defect complex.[23] In other words, a defect may possess a positive binding energy (thermodynamically unstable) but could be kinetically trapped and be present because of the high activation energy for dissociation at a given temperature. The formation of kinetically stabilized defect complexes can occur in a non-equilibrium process such as crystal growth or corrosion. In this paper we focus on the thermodynamically stable defect complexes as these are anticipated to be the predominant in terms of concentration.

We emphasize here based on Sections 2.1 and 2.2 that we will limit the discussion in what follows to the defects in the configurations that have the lowest formation energy and in the charge states that are both physically realizable and thermodynamically stable against dissociation. In this context, ''a thermodynamically stable defect'' means it has a negative binding energy, while ''a stable defect'' indicates that its charge is possible to realize in the simulation cell without delocalization of electrons or holes. In the following, the defects that satisfy both of these definitions are presented. In the ESI† we provide a summary of all the charged defects that will be excluded from the rest of the paper either because they have positive binding energy, or because their charge is not possible to realize, or both.

2.3 Density functional theory calculations

The projector-augmented plane-wave method[45] as implemented in the Vienna Ab-initio Simulation Package (VASP),[46–49] was utilized to perform the density functional theory calculations. The $4s^2\ 4p^6\ 4d^2\ 5s^2$ were treated as valence electrons for zirconium, and the $2s^2\ 2p^4$ were treated as valence electrons for oxygen. Consistent with our previous work on the native defects of tetragonal zirconia,[31] we used a kinetic energy cutoff of 450 eV, a supercell composed

of 2 × 2 × 2 conventional unit cells, and 2 × 2 × 2 Monkhorst–Pack *k*-point mesh. The error in total energy with respect to calculations performed using a kinetic energy cutoff of 600 eV is less than 5 meV per ZrO_2. On the other hand the error in the total energy with respect to calculations performed using a 6 × 6 × 6 *k*-point mesh was found to be less than 1 meV per ZrO_2.

The parameterization of Perdew, Burke, and Ernzerhof (PBE)[50,51] was used to represent the exchange–correlation. The sufficiency of PBE alone without an extra on site Coulomb interaction (DFT + *U*) to describe T-ZrO_2 has been demonstrated recently in the course of studying electron transfer on the surfaces of metal oxides.[52] The choice of standard PBE is also desirable here to allow the investigation of the energetics and the vibrational properties of a wide range of hydrogen defects to compare their relative abundance. This type of investigation becomes computationally prohibitive if one appeals to more accurate *ab initio* methods such as the hybrid functionals. As explained in the Introduction, there is a lack of studies on hydrogen defects in T-ZrO_2 and a comprehensive study is needed to set the ground for future work that can down-select a few of these defects and study them more thoroughly using a higher rung on the Jacob ladder.[53]

In order to understand the effect of the local structure in a crystalline solid on the vibrations of hydrogen and also to provide a computationally derived database that can be validated by Infra-Red and Raman spectroscopy measurements, we calculated the vibrational frequencies for certain hydrogen defects. In particular, whenever a hydroxyl group or a hydrogen molecule is part of a thermodynamically stable defect, we calculated their stretch mode frequency in the harmonic approximation. We targeted these particular species because their stretch mode frequency is known to be much higher than the host vibrational modes and hence justifying fixing the host ions while calculating the vibrational frequencies of hydrogen. The details of the calculations are similar to what is presented in ref. 31 except that we found a finite-difference distance of 0.008 Å is needed to obtain converged frequencies for hydrogen defects in contrast to 0.004 Å used in our study of the native defects. Since anharmonic effects and the limitations inherent in DFT functionals (including hybrids) can significantly affect the absolute values of the vibrational frequencies,[54] it was suggested that, $\Delta\omega$, the difference between the harmonic frequency in the crystalline solid and the harmonic frequency in the gas phase, is a better metric to utilize when comparing with experiments. Thus, the stretch mode of the hydrogen molecule and the hydroxyl group in the solid was referenced to the same mode of these species in the gas phase. Our calculated reference values are 4317 cm^{-1} for H_2 and 3684 cm^{-1} for OH^- in the gas phase. The experimental values (anharmonic) for these modes are 4161 cm^{-1} and 3556 cm^{-1}, respectively.[55,56]

3. Results and discussion

3.1 Defect energetics

In this section we discuss the formation energies of the three categories of hydrogen defects, namely, the interstitial, the complex with an oxygen vacancy, and the complex with a zirconium vacancy in the two limiting cases of oxygen rich (oxidizing) and oxygen poor (reducing) conditions. This is followed by a discussion of the thermodynamic stability of the complexes utilizing the binding energy as a metric.

3.1.1 Formation energies and thermodynamic transition levels. Fig. 2 is a plot of the formation energies of hydrogen defects as a function of the chemical potential of electrons under (a) oxygen poor conditions and (b) oxygen rich conditions. For each defect we show only the predominant charge states.

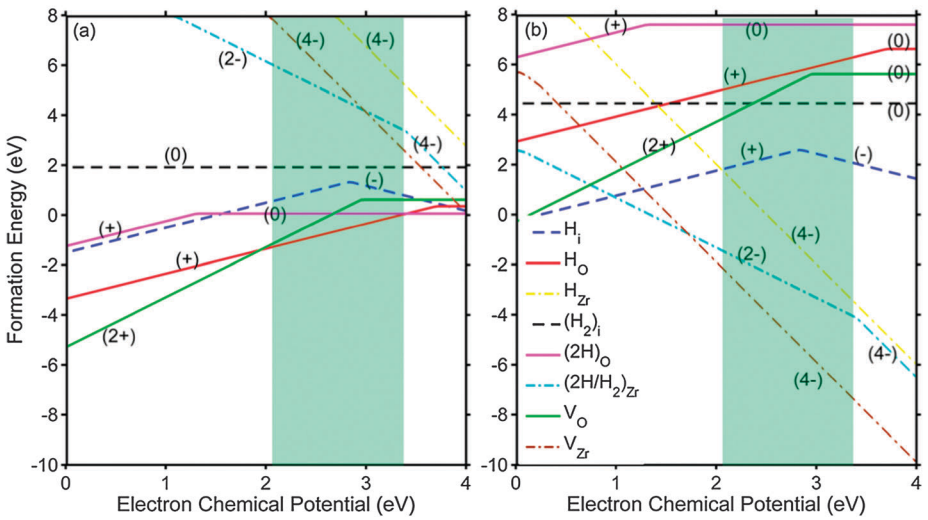

Fig. 2 The formation energy of hydrogen defects under (a) oxygen poor conditions and (b) oxygen rich conditions. The formation energies of oxygen and zirconium vacancies taken from ref. 31 are also shown. Solid, dashed, dot-dashed lines indicate oxygen-related, interstitial, zirconium-related defects, respectively. The shading indicates the range of the chemical potential of electrons accessible by self-doping due to the native defects as determined in ref. 31.

For comparison, we show also the formation energies of oxygen and zirconium vacancies.[31] The shading in the figure indicates the range of the chemical potential of electrons accessible by self-doping due to the native defects of T-ZrO_2 as determined in our previous work.[31] The presence of hydrogen in T-ZrO_2, regarded as an extrinsic dopant, can affect this range. Quantifying the effect of hydrogen on this range requires thermodynamic analysis similar to what is presented in ref. 31 which is not the scope of this work. Thus, the shaded range shown in Fig. 2 has to be regarded as a very probable initial guess for the accessible range in hydrogenated T-ZrO_2. On the other hand, the remaining range of μ_F can also be made accessible by doping with aliovalent cations or anions, making it important to consider the region outside the shading as well. Before discussing the details of Fig. 2, it is important to stress that the thermodynamic transition levels from charge q_1 to charge q_2 or each defect are independent of the chemical potentials of species. Hence, in the discussion we will quote the values of these levels. On the other hand, the range of μ_F over which certain defects predominate over the others depends on the chemical potential of species. Fig. 2 depicts only the two extremes of μ_O (poor and rich) and the rich extreme of μ_H. Hence, it is not that meaningful to quote in the discussion exact ranges of μ_F over which predomination of certain defect takes place. We will thus limit the discussion of predomination to qualitative trends. It is straightforward, however, to derive from Fig. 2 quantitative ranges of predomination at specific values of the chemical potential of species when desired.

Our calculations indicate that interstitial hydrogen, H_i, exhibits a negative-*U* behavior with a *U* value of −1.96 eV. Moreover, the interstitial hydrogen defect was found to be amphoteric, *i.e.*, it can exist both as a hydride ion and as a proton in distinct ranges of μ_F. The thermodynamic transition level (+/−) for interstitial hydrogen from the proton to the hydride ion happens to be at 2.84 eV which is within the range of μ_F accessible by self-doping due to the native defects. Recently, it was also shown that interstitial hydrogen is both amphoteric and a negative-*U* defect in monoclinic zirconia.[21] A further confirmation of the negative *U*-behavior is evident from the atomic and electronic structure of interstitial hydrogen defects discussed in Section 3.2. The interstitial hydrogen molecule, $(H_2)_i$, is predominantly neutral and has higher formation energy compared to the interstitial mono-hydrogen.

The charge state (+) is predominant for the defect complex made of a mono-hydrogen and an oxygen vacancy, H_O, in almost all the band gaps except for a narrow range close to the conduction band where the neutral charge state predominates. This behavior for this defect was found recently in monoclinic ZrO_2 and HfO_2.[21] However, in another n-type oxide (ZnO) only the charge state (+) was found to be dominant,[2] while in a p-type oxide (Cu_2O) each of the charge states (−,0,+) was found to predominate a certain region of the band gap.[27] We also found that upon inserting another hydrogen species in the oxygen vacancy site to form $(2H)_O$, the formation energy of the complex increases compared to that of H_O (except for a narrow range of μ_F under the oxygen poor conditions). The tendency of the oxygen vacancy to reject hydrogen clustering was also observed in ZnO and MgO.[2] Contrary to the mono-hydrogen case, the neutral charge state of the complex of two hydrogen and an oxygen vacancy, $(2H)_O$ is predominant in most of the band gap except for a range of 1.3 eV near the valence band where the (+) charge state predominates.

The predominant charge state for the complex made of a mono-hydrogen and a zirconium vacancy, H_{Zr}, is (4−) and indeed it is the only thermodynamically stable charge state. Interestingly adding another hydrogen species into the zirconium vacancy to form $(2H/H_2)_{Zr}$ lowers the formation energy of the complex compared to that of H_{Zr} and in this case multiple charge states are thermodynamically stable. The charge state (2−) predominates starting from the valence band edge up to the thermodynamic transition level (2−/4−) at 3.4 eV. A similar tendency for hydrogen accumulation in cation vacancies was also observed in Al_2O_3.[39] This accumulation can take place in a non-equilibrium process such as crystal growth[24] or corrosion. The abundance of the clusters formed in this process depends on the formation energy of these clusters. Once equilibrium is reached in the region in which hydrogen clusters were formed, the binding energy would be the metric to decide their thermodynamic stability. Quantifying the abundance, thermodynamic stability and electronic structure of these complexes is of paramount importance to assess the resistance of the oxide layers natively grown on metal surfaces to the deleterious effects of hydrogen. Hydrogen is known to interact strongly with the host lattice[26] and can lead to bond breaking subsequently followed by degradation of the mechanical properties of the host. While this effect is well-studied in metals and is commonly termed as hydrogen embrittlement,[1] it is by far less studied in oxides. The fact that two hydrogen species in a zirconium vacancy have lower formation compared to the case of mono-hydrogen led us to investigate two special cases where three or four hydrogen species accumulate in a zirconium vacancy. These two cases are discussed later.

Fig. 2 contrasts the predominant hydrogen defects under oxygen poor and oxygen rich conditions. In the former case (Fig. 2(a)), mono-hydrogen associated with an oxygen vacancy, H_O, in the charge state (+) predominates for most of the band gap except for a narrow range close to the conduction band in which the di-hydrogen oxygen vacancy complex, $(2H)_O$, in the neutral charge state predominates. Under the oxygen rich conditions (Fig. 2(b)) and starting from the valence band edge, the interstitial proton predominates over a range of μ_F. For the rest of the band gap and up to the conduction band edge, the di-hydrogen associated with a zirconium vacancy, $(2H/H_2)_{Zr}$, predominates first in the charge state (2−) and then in the charge state (4−). Our results under the oxygen poor conditions are consistent with the experimental findings of Park and Olander.[15] They observed that under oxygen poor (reducing) conditions, the solubility of hydrogen increases with the increase of the off-stoichiometry, *x*, in T-ZrO_{2-x} in accordance with our finding that hydrogen associates with oxygen vacancies under these conditions.

We examined the clustering of 3H and 4H in a zirconium vacancy in the charge states (−) and (0), respectively. The choice of these particular charge states is justified in the atomic and electronic structure Section 3.2. In Fig. 3 we present all the zirconium related defects under oxygen poor (a) and oxygen

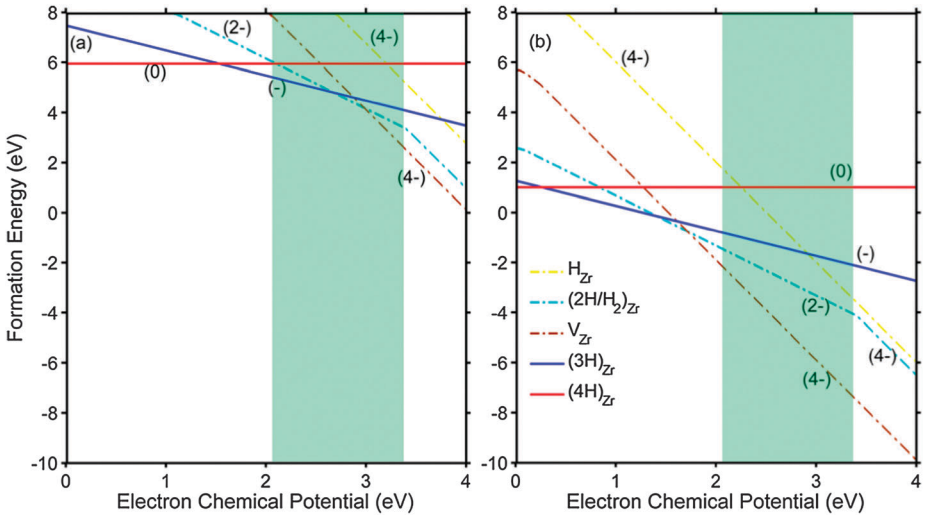

Fig. 3 The formation energy of hydrogen defect complexes with a zirconium vacancy including the two special clusters that contain 3H and 4H under (a) oxygen poor conditions and (b) oxygen rich conditions. The formation energy of the zirconium vacancy is included for comparison. The shading indicates the range of the chemical potential of electrons accessible by self-doping due to the native defects as determined in ref. 31.

rich conditions (b). It is clear from the figure that the clusters $(3H)'_{Zr}$ and $(4H)^{\times}_{Zr}$ predominate the hydrogen–zirconium vacancy complexes in certain ranges of μ_F mainly in the p-type region. Under the oxygen rich conditions these clusters have low formation energies. This demonstrates that zirconium vacancies can act as trapping sites for hydrogen and the resulting complexes can be precursors for the adverse effects of hydrogen on the mechanical stability of the oxide. Furthermore, as we show below, most of the hydrogen–zirconium vacancy complexes have high binding energy.

3.1.2 Binding energies. The calculated binding energies for the thermodynamically stable complexes are reported in Table 1. Although in our classification of the defects presented above we regarded the interstitial hydrogen molecule as an elementary defect, it is also possible to consider it as a complex formed due to association between a proton and a hydride ion. Assuming the latter picture, we found it to be stable against dissociation with a binding energy of −0.74 eV. The predominant mono-hydrogen oxygen vacancy complex charge state identified above is (+) and this indeed is a highly stable complex with a binding energy −2.22 eV. For this complex, the calculation of the binding energy for the charge states (2+) and (0) according to our definition is problematic. The only possible dissociation pathways for those two charge states involve the formation of a disallowed charge state for a negative-*U* defect (that is the singly charged oxygen vacancy and neutral interstitial hydrogen). We reported in the table values calculated upon relaxing the constraint of discarding the negative-*U* disallowed charge states. Thus, $H^{\bullet\bullet}_O$ was deemed to be unstable, while $H^{\times}_O$ was found to be stable with a binding energy of −1.5 eV. On the other hand, the calculated binding energies for the di-hydrogen oxygen vacancy complexes indicate relatively shallow binding. We found the easiest dissociation pathway for these complexes to involve the formation of $H^{\bullet}_O$.

Table 1 The binding energy of the thermodynamically stable hydrogen defect complexes

Complex	Binding energy (eV)
$(H_2)_i^{\times}$	−0.74
$H^{\bullet\bullet}_O, H^{\bullet}_O, H^{\times}_O, H'_O$	+0.59,[a] −2.22, −1.5,[a] −0.74
$(2H)^{\bullet}_O, (2H)^{\times}_O, (2H)'_O$	−0.09, −0.76, −0.78
H'''_{Zr}	−1.28
$(2H)^{\times}_{Zr}, (2H)'_{Zr}, (2H)''_{Zr}, (H_2)''''_{Zr}$	−2.65, −2.79, −2.94, −1.06
$(3H)'_{Zr}, (4H)^{\times}_{Zr}$	−1.17, −0.02

[a] The only possible dissociation pathways for these complexes involve the formation of a disallowed charge state for a negative-*U* defect. Here we report the values computed based on eqn (2) but by relaxing the constraint related to the negative-*U* defects.

Only the charge state (4−) is stable thermodynamically for the mono-hydrogen zirconium vacancy complex, H_{Zr}, with a binding energy of −1.28. For the di-hydrogen zirconium vacancy complex, the predominant charge states $(2H)''_{Zr}$ and $(H_2)''''_{Zr}$ have binding energies of −2.79 eV and −1.06 eV, respectively. The latter charge state is the only one in which the hydrogen molecule exists as an entity in the vacant site. The cluster of 3H and zirconium vacancy, $(3H)'_{Zr}$, was found to be stable with a binging energy of −1.17 eV, while the cluster formed between 4H and a zirconium vacancy, $(4H)^{\times}_{Zr}$, has a very shallow binding energy of −0.02 eV. The limiting dissociation pathway of the $(4H)^{\times}_{Zr}$ cluster is the one that leads to the formation of the $(3H)'_{Zr}$ cluster and an interstitial proton.

To reiterate, clustering of hydrogen in zirconium vacancies can lead to the formation of thermodynamically stable defects, a result of significant importance for the mechanical properties of oxides.

3.2 Defect atomic and electronic structures

Understanding the defect atomic and electronic structure is of utmost importance. On one hand it can help in rationalizing

many of the energy-based results. On the other hand it provides a basis for fundamental measurable quantities that can be probed experimentally such as the net spin of a defect that can be probed in muon spectroscopy[16] and characteristic vibrational frequencies that can be detected in Raman and Infra Red spectroscopy.[57] In this section, we discuss the atomic and electronic structure of each of the three categories of hydrogen defects. In particular, for each category we examine the geometry of the minimum energy configuration of each defect. In addition, we utilize the net spin density and Bader charge analysis as metrics to understand the electron distribution within the defect. This analysis is complemented by examining the stretch mode frequency of any hydroxyl group or hydrogen molecule that resides as an entity within the defect. As discussed in Section 2.3 we report the difference, $\Delta\omega$, between the harmonic stretch of the species in the condensed phase and the harmonic stretch of the reference (OH^- or H_2) in the gas phase. For comparison purpose, we report here that our calculated O–H and H–H bond lengths in the gas phase OH^- and H_2 are 0.977 Å and 0.751 Å, respectively. For each of the upcoming figures, the color code and the orientation of the simulation cell is the same as in Fig. 1.

3.2.1 Interstitial defects. Fig. 4 depicts the minimum energy configuration for the possible charge states of interstitial mono-hydrogen (a–c) and interstitial hydrogen molecule (d and e). An isosurface of the net electronic spin density is also shown whenever the defect exhibits a net magnetic moment. Closely related to Fig. 4 is Table 2 in which we present the calculated Bader charges, the bond length of any OH^- or H_2 species and the quantity $\Delta\omega$ defined above.

The underlying structure for both the charge states (+) and (0) of interstitial mono-hydrogen is a hydroxyl group formed between hydrogen and one of the lattice oxygens and oriented in ⟨111⟩. The same structure was also identified through DFT calculations on T-ZrO_2 in ref. 6. Furthermore, we found that the net spin localized on the defect in the case of the neutral charge state is zero, indicating that the 1s electron of the hydrogen atom is in a shallow electronic state right at the edge of the conduction band. This was also found to be the case in monoclinic zirconia through electronic density of states calculations.[58] Thus, in the neutral DFT simulation cell the hydrogen is indeed a proton and most of the 1s electron wave function is delocalized. This is supported by the very similar Bader charge, O–H bond length, and $\Delta\omega$ for (+) and (0) cases. This also is in accordance with the negative-U behavior identified through the energetics in Section 3.1.1. A general feature that we observe for all the OH^- groups that arise in the hydrogen defects in T-ZrO_2 is the reduction of the stretch frequency (*e.g.* -279 cm^{-1} for the interstitial proton) compared to the gas phase OH^-. This is an important signature that is amenable to investigation in Raman and Infra Red spectroscopy experiments. A more striking feature was identified for H_2 vibrations and is discussed below.

Table 2 Calculated properties for the interstitial hydrogen defects. Bader charges are shown for hydrogen only. The distance, d, is the bond length of H_2 or OH^- if either of them was detected in the simulation cell. The frequency difference, $\Delta\omega$, is defined in Section 2.3

Defect	Bader charge (e)	d (Å)	$\Delta\omega$ (cm^{-1})
$H_i^{\bullet}$	+0.62	O–H: 0.986	-279^a
$H_i^{\times}$	+0.61	O–H: 0.987	-310^a
$H_i^{'}$	−0.49	—	—
$(H_2)_i^{\times}$	−0.11, +0.04	H–H: 0.739	$+84^b$
$(H_2)_i^{'}$	−0.14, −0.01	H–H: 0.786	-825^b

[a] The reference is the stretch mode of OH^-. [b] The reference is the stretch mode of H_2.

The favorable site for the hydride ion was found to be the octahedral site as shown in Fig. 4(c). This is expected given the electrostatic repulsion between the eight oxygen ions in the conventional unit cell and the hydride ion. The zero net spin on the defect and the negative Bader charge both indicate the pairing between two 1s electrons on the interstitial hydrogen and confirm its character as a hydride ion.

The neutral interstitial hydrogen molecule was found to be oriented in the ⟨001⟩ direction as depicted in Fig. 4(d). The bond length of the interstitial molecule is shortened by 0.012 Å and the stretch mode frequency is enhanced by +84 cm^{-1} compared to the gas phase. Our calculations indicate that this is a general feature for all the neutral hydrogen molecules that arise in a defect in T-ZrO_2. This is strikingly the opposite of what was found for the interstitial hydrogen molecule in semiconductors both experimentally and theoretically.[54] The shortening of the bond length of the molecule and the upshift of its vibrational frequency are the signature of enhanced intramolecular interaction. Such enhancement of the intramolecular interactions for a molecule due to the intermolecular interactions in the condensed phase is counterintuitive.[59] We believe that this important finding requires future experimental confirmation. We also found that the di-hydrogen anion is stable in the crystalline environment of T-ZrO_2 in the ⟨100⟩ direction. The extra electron added to $(H_2)_i^{\times}$ to form $(H_2)_i^{'}$ is mainly shared among the surrounding zirconium cations as

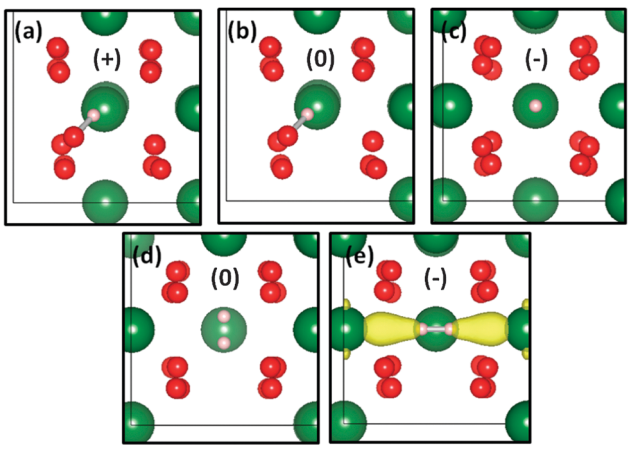

Fig. 4 The minimum energy structures of the thermodynamically stable interstitial hydrogen defects together with an isosurface for the net spin density (if nonzero). (a) $H_i^{\bullet}$, (b) $H_i^{\times}$, (c) $H_i^{'}$, (d) $(H_2)_i^{\times}$, and (e) $(H_2)_i^{'}$. The yellow isosurface is taken at 0.01 $Å^{-3}$.

indicated by the net spin density in Fig. 4(e) and the Bader charge analysis. On the other hand, the di-hydrogen cation was found to be unstable in the crystalline environment of T-ZrO_2. Our findings related to the di-hydrogen anion and cation are consistent with what is generally known about these molecular ions, *i.e.*, the former is stable in a condensed phase but not in the gas phase while the converse applies for the latter.[60]

3.2.2 Hydrogen–oxygen vacancy complexes. The key to understand the structure of hydrogen–oxygen vacancy complexes is to recall the electronic structure of the oxygen vacancy identified previously.[31,61] The latter was found to have a negative-*U* character. In addition, it was found that the neutral oxygen vacancy has the electronic structure of an F-center where two d-electrons from the neighboring zirconium ions localize on the vacant site. Removing one of these electrons to create a singly charged vacancy leads to the localization of the remaining electron right on the vacant site. Removing the last electron leads to the formation of the doubly charged oxygen vacancy. In Fig. 5 we show the minimum energy configuration for the possible charge states of the complexes formed between the oxygen vacancy and the mono hydrogen (a–c), and between the oxygen vacancy and the di-hydrogen (d–f). Whenever a defect exhibits a net magnetic moment, an isosurface of the net spin density is also shown. In Table 3 we present the calculated Bader charges for the hydrogen species associated with the oxygen vacancy and the distance between the two hydrogen species if they coexist in the vacant site. This distance is not a bond length, because we did not detect any chemically bonded species when hydrogen associates with an oxygen vacancy. Thus, we did not calculate the vibrational frequencies of hydrogen in oxygen vacancies as the lack of chemical bonding leads to severe reduction in its frequencies. This reduction makes hydrogen vibrations not very distinguishable from the host vibrations.

The thermodynamically stable most positive charge state for the mono-hydrogen oxygen vacancy complex is (+). The association results in a hydride ion located almost at the center of a doubly charged oxygen vacancy as shown in Fig. 5(a). Bader charge analysis also supports that the hydrogen species in this case is a hydride ion. This charge state was found to be energetically predominant for most of the band gap of T-ZrO_2. Adding one more electron to obtain the charge state (0) leads to the localization of this electron in the d orbitals of two neighboring zirconium ions at the edge of the conduction band minimum as shown in Fig. 5(b). This structure is akin to the so-called multicenter bond configuration for hydrogen in the oxygen vacancy in metal oxides.[2] The charge state (−) is obtained by adding one more electron, the resultant is a hydride ion associated with an F-center. The strong repulsion between the two electrons of the F-center and the hydride ion renders this charge state very unfavorable energetically.

Table 3 Calculated properties for the hydrogen oxygen vacancy complexes. Bader charges are shown for hydrogen only. The distance, *d*, is between two hydrogen species and does not correspond to a bond length

Defect	Bader charge (*e*)	*d* (Å)
$H_O^{\bullet}$	−0.59	—
$H_O^{\times}$	−0.66	—
$H_O^{'}$	−0.76	—
$(2H)_O^{\bullet}$	−0.24, −0.19	0.984
$(2H)_O^{\times}$	−0.50, −0.52	1.928
$(2H)_O^{'}$	−0.55, −0.56	2.071

We did not find any evidence that the hydrogen molecule can exist in an oxygen vacancy in T-ZrO_2. Thus, any two hydrogen species in an oxygen vacancy are not bonded together; instead they exist as an oriented dumbbell. We found that this dumbbell is favorably oriented in the ⟨110⟩ direction for all the charge states. The thermodynamically stable most positive charge state for two hydrogen species in an oxygen vacancy is (+). The structure of this complex, shown in Fig. 5(d), consists of two hydrogen atoms separated by a distance of 0.984 Å associated with a singly charged oxygen vacancy. The charge density of the electron of the singly charged vacancy is spread over the two hydrogen atoms and the surrounding oxygen and zirconium ions. The distance between the two hydrogen atoms is significantly larger than the bond length of the hydrogen molecule or even the di-hydrogen anion (compare with Table 2). The charge state (0) of the complex, shown in Fig. 5(e), consists of two hydride ions associated with a doubly charged oxygen vacancy. The partial charges on the two hydrogen species confirm their identification as hydride ions. Finally, obtaining the charge state (−) by adding one further electron leads to its localization on the d orbitals of two neighboring zirconium cations as shown in Fig. 5(f). The strong repulsion between the two hydride ions and the extra localized electron elongated the H–H distance to 2.071 Å and renders the charge state energetically unfavorable, but still thermodynamically stable.

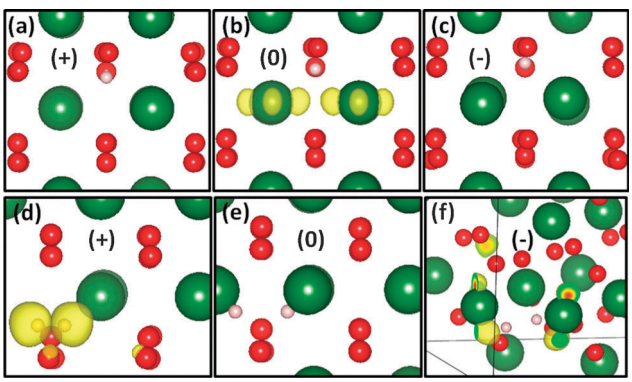

Fig. 5 The minimum energy structures of the thermodynamically stable hydrogen–oxygen vacancy complexes together with an isosurface for the net spin density (if nonzero). (a) $H_O^{\bullet}$, (b) $H_O^{\times}$, (c) $H_O^{'}$, (d) $(2H)_O^{\bullet}$, (e) $(2H)_O^{\times}$, and (f) $(2H)_O^{'}$. The yellow isosurface is taken at 0.01 $Å^{-3}$.

3.2.3 Hydrogen–zirconium vacancy complexes. Before discussing hydrogenated zirconium vacancies, we recall the electronic structure of pristine ones that we identified previously.[31] The neutral zirconium vacancy has the V-center structure where the vacant site is surrounded by four holes localized on four neighboring oxygen ions. By filling the four holes with electrons one by one, we obtain all the possible charge states until filling all of them and obtaining $V_{Zr}^{''''}$.

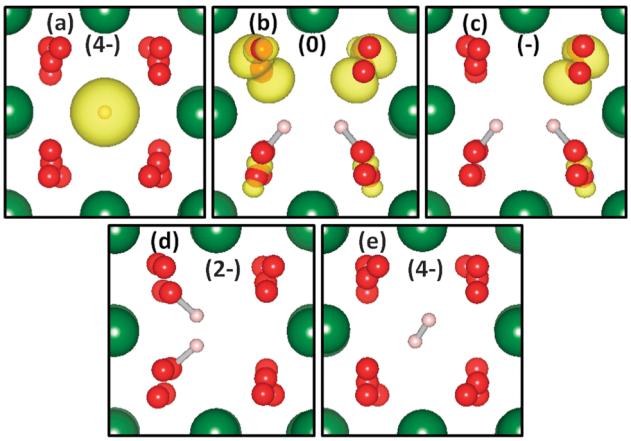

Fig. 6 The minimum energy structures of the thermodynamically stable hydrogen–zirconium vacancy complexes together with an isosurface for the net spin density (if nonzero). (a) $H_{Zr}^{''''}$, (b) $(2H)_{Zr}^{\times}$, (c) $(2H)_{Zr}^{'}$, (d) $(2H)_{Zr}^{''}$, and (e) $(H_2)_{Zr}^{''''}$. The yellow isosurface is taken at 0.01 Å^{-3}.

Table 4 Calculated properties for hydrogen–zirconium vacancy complexes. Bader charges are shown for hydrogen only. The distance, d, is the bond length of H_2 or OH^- if either of them was detected in the simulation cell. The frequency difference, $\Delta\omega$, is defined in Section 2.3

Defect	Bader charge (e)	d (Å)	$\Delta\omega$ (cm^{-1})
$(H)_{Zr}^{''''}$	+0.04	—	—
$(2H)_{Zr}^{\times}$	+0.63, +0.63	O–H: 0.974, 0.974	−120, −130[a]
$(2H)_{Zr}^{'}$	+0.62, +0.62	O–H: 0.975, 0.975	−91, −103[a]
$(2H)_{Zr}^{''}$	+0.62, +0.62	O–H: 0.977, 0.977	−56, −71[a]
$(H_2)_{Zr}^{''''}$	−0.04, +0.03	H–H: 0.738	+145[b]

[a] The reference is the stretch mode of OH^-. [b] The reference is the stretch mode of H_2.

The latter was reckoned to be the predominant energetically. Fig. 6 shows the minimum energy configuration for all the possible and thermodynamically stable charge states for the hydrogenated zirconium vacancies. An isosurface of the net spin density is shown whenever a defect exhibits a net magnetic moment. Table 4 shows the calculated Bader charge for hydrogen in zirconium vacancies, and the bond length and $\Delta\omega$ for any OH^- or H_2 species in the defect.

For the defect complex made of a mono-hydrogen and a zirconium vacancy, only the (4−) charge state is thermodynamically stable. The atomic and electronic structure of this defect depicted in Fig. 6(a) reveals that hydrogen in atomic form is located at the center of $V_{Zr}^{''''}$. The spherically symmetric net spin density of the 1s electron localized on hydrogen is clearly observed. The key to comprehend hydrogen molecule–zirconium vacancy interactions is the following rule that we deduced from our DFT simulations. The priority is to fill the holes localized on the oxygen ions surrounding the zirconium vacancy. This is accomplished by dissociating the H_2 molecule and donating its two electrons to fill the holes. The resulting two protons bind to two of the surrounding oxygens to form hydroxyl groups. Upon filling all the holes, the H_2 molecule can be stabilized in the vacant site. With this rule in mind we observe in Fig. 6(b) that the association between H_2 and $V_{Zr}^{\times}$ leads to the dissociation of the molecule, filling two holes on two oxygen ions, forming two OH^- groups between the resulting two protons and the two hole-free oxygen ions, and finally leaving two holes localized on other two oxygen ions. Adding one electron to obtain the charge state (−) leads to filling one more hole as in Fig. 6(c). Adding one further electron fills the last hole and leads to the charge state (2−) shown in Fig. 6(d). This charge state is the one that predominates energetically for a wide range in the band gap of T-ZrO_2 as discussed in Section 3.1.1. At this stage trying to add one more electron to obtain the charge state (3−) does not lead to the localization of the electron on the defect. The reason is that no more holes are available for recombination and also the di-hydrogen cation cannot be stabilized in the condensed environment of T-ZrO_2 as mentioned above. Thus, the charge state (3−) cannot be realized. However, the charge state (4−) is possible where the last added two electrons lead to the formation of the H_2 molecule in the vacant site with ⟨111⟩ orientation being the most favorable as shown in Fig. 6(e). The Bader charge analysis supports the arguments presented above, where all the identified protons have a partial charge of about +0.6e and all the neutral species (H_2 and H) have an almost zero partial charge as shown in Table 4. Also in accordance with what we identified earlier, the stretch frequency of any OH^- associated with zirconium vacancy is red-shifted while that of the H_2 molecule associated with zirconium vacancy is blue-shifted.

The rule identified above for the di-hydrogen interaction with a zirconium vacancy is what guided our choice to examine the charge states (−) and (0) for the 3H and 4H, respectively. Consider the neutral zirconium vacancy with 4 holes surrounding the vacant site as the starting point. Inserting 3H leads to filling three holes and forming three OH^- groups between the resultant protons and hole-free oxide ions. Given that hole localization on the oxide ion is not favored by the Madelung potential of the oxide,[62] we decided to the fill the last hole with an electron and hence considering the charge state (−). In the case of 4H, the electrons provided by the hydrogen species are enough to fill all the holes and eventually forming four OH^- groups. However, it seems that the repulsion between the four protons is strong such that the binding energy of this complex is only −0.02 eV. Fig. 7 shows the relaxed structure for these two special clusters. In Table 5 we report the calculated Bader charge for the hydrogen species together with the bond lengths

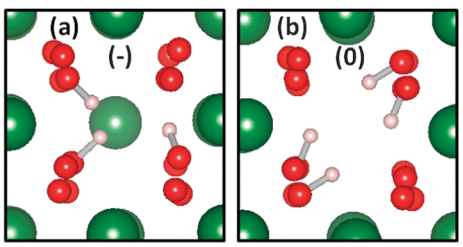

Fig. 7 The relaxed structures of the clusters (a) $(3H)_{Zr}^{'}$, and (b) $(4H)_{Zr}^{\times}$.

Table 5 Calculated properties for the two special clusters formed between hydrogen and the zirconium vacancy. Bader charges are shown for hydrogen only. The distance, d, is the bond length of the OH^- detected in the defect. The frequency difference, $\Delta\omega$, is defined in Section 2.3

Defect	Bader charge (e)	d (Å)	$\Delta\omega$ (cm^{-1})
$(3H)'_{Zr}$	+0.61, +0.63, +0.62	O–H: 0.973, 0.982, 0.991	−51, −239, −450[a]
$(4H)^{\times}_{Zr}$	+0.64, +0.64, +0.62, +0.62	O–H: 0.979, 0.979, 0.996, 0.996	−181, −188, −489, −494[a]

[a] The reference is the stretch mode of OH^-.

and the vibrational frequencies for the hydroxyl groups. Bader charge analysis confirms that all the hydrogen species in these two clusters are protons. In addition to this, the vibrational frequencies of all the OH^- groups are downshifted conforming to the trend we identified for all OH^- in T-ZrO_2.

4. Conclusion

The energy-structure paradigm was adopted to study hydrogen defects in tetragonal ZrO_2 by means of density functional theory simulations. Defect energies were analyzed by two metrics; the formation energy and a thorough formulation of the binding energy of a defect complex. The atomic and electronic structures of the defects were examined utilizing Bader charge analysis, shifts in the vibrational frequencies and the DFT-calculated relaxed geometries and net spin densities.

Our results indicate that under oxygen poor conditions and for most of the values of the chemical potential of electrons, the predominant form of hydrogen defects is $H^{\bullet}_{O}$. $H^{\bullet}_{O}$ is a complex formed by the association of a hydride ion and a doubly charged oxygen vacancy. This complex is very stable thermodynamically with a binding energy of −2.22 eV. Furthermore, this observation is consistent with the proportionality between hydrogen solubility and the degree of hypostoichiometry observed experimentally under oxygen poor conditions. Under oxygen rich conditions several hydrogen defects predominate depending on the chemical potential of electrons. Starting from the edge of the valence band and toward the edge of the conduction band these are interstitial protons, then the complex $(2H)''_{Zr}$, and finally for the rest of the band gap, the complex $(H_2)''''_{Zr}$. The latter two complexes are thermodynamically stable with binding energies of −2.94 eV and −1.06 eV, respectively. In $(2H)''_{Zr}$ the two hydrogen species exist in the zirconium vacancy in the form of hydroxyl groups, while in $(H_2)''''_{Zr}$ they exist as a hydrogen molecule.

We found out that zirconium vacancies have a tendency to act as hydrogen accumulators up to three hydrogen species per vacancy. This tendency of cation vacancies can be a precursor for the degrading effect of hydrogen on the mechanical properties of T-ZrO_2 and the metal oxides in general.

Finally, in order to assist future experimental detection of hydrogen defects in T-ZrO_2, we calculated the shifts in the vibrational frequencies of hydroxyl groups and hydrogen molecules that can arise as hydrogen defects in T-ZrO_2 taking their gas phase frequencies as reference. Without exception, we observed that all the hydroxyl groups experience a red-shift while all the hydrogen molecules experience a blue-shift in tetragonal zirconia.

We believe that the comprehensive study presented here concerning hydrogen defects in T-ZrO_2 is a major milestone in our understanding of technologically important phenomena such as hydrogen pickup in zirconium alloys in nuclear reactors, the low temperature degradation of zirconia ceramics in biomedical applications, and the adverse effects of hydrogen on zirconia gate dielectrics.

Acknowledgements

This research was supported by the Consortium for Advanced Simulation of Light Water Reactors (CASL), an Energy Innovation Hub for Modeling and Simulation of Nuclear Reactors under U.S. Department of Energy Contract No. DE-AC05-00OR22725. We acknowledge the National Science Foundation for computational support through the XSEDE Science Gateways program with the research allocation (TG-DMR120025). All the atomistic visualizations were generated using the software VESTA.[63]

References

1 J. Song and W. A. Curtin, *Nat. Mater.*, 2013, **12**, 145.
2 A. Janotti and C. G. Van de Walle, *Nat. Mater.*, 2007, **6**, 44.
3 G. A. Jeffrey, *An Introduction to Hydrogen Bonding*, Oxford University Press, New York, 1997.
4 A. Yilmazbayhan, E. Breval, A. T. Motta and R. J. Comstock, *J. Nucl. Mater.*, 2006, **349**, 265.
5 A. Chroneos, B. Yildiz, A. Tarancon, D. Parfitt and J. Kilner, *Energy Environ. Sci.*, 2011, **4**, 2774.
6 A. L. Shluger, A. Foster, J. L. Gavartin and P. V. Sushko, in *Nano and Giga Challenges in Microelectronics*, ed. J. Greer, A. Korkin and J. Labanowski, Elsevier, Amsterdam, 2003.
7 B. Cales, *Clin. Orthop. Relat. Res.*, 2000, **379**, 94.
8 X. Guo, *Chem. Mater.*, 2004, **16**, 3988.
9 J. Chevalier, L. Gremillard, A. V. Virkar and D. R. Clarke, *J. Am. Ceram. Soc.*, 2009, **92**, 1901.
10 B. Cox, *J. Nucl. Mater.*, 2005, **336**, 331.
11 B. Cox, *J. Nucl. Mater.*, 1999, **264**, 283.
12 J. Kang, E.-C. Lee, K. J. Chang and Y.-G. Jin, *Appl. Phys. Lett.*, 2004, **84**, 3894.
13 G. D. Wilk, R. M. Wallace and J. M. Anthony, *J. Appl. Phys.*, 2001, **89**, 5243.
14 T. Smith, *J. Nucl. Mater.*, 1966, **18**, 323.
15 K. Park and D. R. Olander, *J. Am. Ceram. Soc.*, 1991, **74**, 72.

16 S. F. J. Cox, J. L. Gavartin, J. S. Lord, S. P. Cottrel, J. M. Gil, H. V. Alberto, J. P. Duarte, R. C. Vilao, N. A. d. Campos, D. J. Keeble, E. A. Davis, M. Charlton and D. P. v. d. Werf, *J. Phys.: Condens. Matter*, 2006, **18**, 1079.
17 R. Nazarov, T. Hickel and J. Neugebauer, *Phys. Rev. B: Condens. Matter Mater. Phys.*, 2010, **82**, 224104.
18 U. Aydin, L. Ismer, T. Hickel and J. Neugebauer, *Phys. Rev. B: Condens. Matter Mater. Phys.*, 2012, **85**, 155144.
19 H. Wang, A. Chroneos, C. Jiang and U. Schwingenschlogl, *Phys. Chem. Chem. Phys.*, 2013, **15**, 7599–7603.
20 P. A. Burr, S. T. Murphy, S. C. Lumley, M. R. Wenman and R. W. Grimes, *J. Nucl. Mater.*, 2013, **443**, 502–506.
21 J. L. Lyons, A. Janotti and C. G. Van de Walle, *Microelectron. Eng.*, 2011, **88**, 1452.
22 B. Malki, O. L. Bacq and A. Pasturel, *J. Nucl. Mater.*, 2011, **416**, 362.
23 J. B. Varley, H. Peelaers, A. Janotti and C. G. Van de Walle, *J. Phys.: Condens. Matter*, 2011, **23**, 334212.
24 C. G. Van de Walle, *Phys. Rev. B: Condens. Matter Mater. Phys.*, 1997, **56**, R10020.
25 C. G. Van de Walle, *Phys. Rev. Lett.*, 2000, **85**, 1012.
26 C. G. Van de Walle and J. Neugebauer, *Nature*, 2003, **423**, 626.
27 D. O. Scanlon and G. Watson, *Phys. Rev. Lett.*, 2011, **106**, 186403.
28 M.-H. Du and K. Biswas, *Phys. Rev. Lett.*, 2011, **106**, 115502.
29 Ç. Kılıç and A. Zunger, *Appl. Phys. Lett.*, 2002, **81**, 73.
30 A. G. Marinopoulos, *Phys. Rev. B: Condens. Matter Mater. Phys.*, 2012, **86**, 155144.
31 M. Youssef and B. Yildiz, *Phys. Rev. B: Condens. Matter Mater. Phys.*, 2012, **86**, 144109.
32 J.-P. Crocombette, D. Torumba and A. Chartier, *Phys. Rev. B: Condens. Matter Mater. Phys.*, 2011, **83**, 184107.
33 J. L. Gavartin, D. M. Ramo, A. L. Shluger, G. Bersuker and B. H. Lee, *Appl. Phys. Lett.*, 2006, **89**, 082908.
34 A. M. Stoneham, J. Gavartin, A. L. Shluger, A. V. Kimmel, D. M. Ramo, H. M. Rønnow, G. Aeppli and C. Renner, *J. Phys.: Condens. Matter*, 2007, **19**, 255208.
35 D. Shrader, S. M. Khalil, T. Gerczak, T. R. Allen, A. J. Heim, I. Szlufarska and D. Morgan, *J. Nucl. Mater.*, 2011, **408**, 257.
36 F. Oba, A. Togo, I. Tanaka, J. Paier and G. Kresse, *Phys. Rev. B: Condens. Matter Mater. Phys.*, 2008, **77**, 245202.
37 R. F. W. Bader, *Chem. Rev.*, 1991, **91**, 893.
38 W. Tang, E. Sanville and G. Henkelman, *J. Phys.: Condens. Matter*, 2009, **21**, 084204.
39 S. N. Rashkeev, K. W. Sohlberg, S. Zhuo and S. T. Pantelides, *J. Phys. Chem. C*, 2007, **111**, 7175.
40 C. G. Van de Walle and J. Neugebauer, *J. Appl. Phys.*, 2004, **95**, 3851.
41 G. Makov and M. C. Payne, *Phys. Rev. B: Condens. Matter Mater. Phys.*, 1995, **51**, 4014.
42 A. Dwivedi and A. N. Cormack, *Philos. Mag. A*, 1990, **61**, 1.
43 D. Fischer and A. Kersch, *Appl. Phys. Lett.*, 2008, **92**, 012908.
44 C. W. M. Castleton, A. Höglund and S. Mirbt, *Phys. Rev. B: Condens. Matter Mater. Phys.*, 2006, **73**, 035215.
45 G. Kresse and J. Joubert, *Phys. Rev. B: Condens. Matter Mater. Phys.*, 1999, **59**, 1758.
46 G. Kresse and J. Hafner, *Phys. Rev. B: Condens. Matter Mater. Phys.*, 1993, **47**, 558.
47 G. Kresse and J. Hafner, *Phys. Rev. B: Condens. Matter Mater. Phys.*, 1994, **49**, 14251.
48 G. Kresse and J. Futhmüller, *Comput. Mater. Sci.*, 1996, **6**, 15.
49 G. Kresse and J. Futhmüller, *Phys. Rev. B: Condens. Matter Mater. Phys.*, 1996, **54**, 11169.
50 J. P. Perdew, K. Burke and M. Ernzerhof, *Phys. Rev. Lett.*, 1996, **77**, 3865.
51 J. P. Perdew, K. Burke and M. Ernzerhof, *Phys. Rev. Lett.*, 1997, **78**, 1396.
52 J. C. Garcia and N. A. Deskins, *J. Phys. Chem. C*, 2012, **116**, 16573–165581.
53 J. P. Perdew, *MRS Bull.*, 2013, **38**, 743.
54 C. G. Van de Walle and J. P. Goss, *Mater. Sci. Eng., B*, 1997, **58**, 17.
55 B. P. Stoicheff, *Can. J. Phys.*, 1957, **35**, 730.
56 J. C. Owrutsky, N. H. Rosenbaum, L. M. Tack and R. J. Saykally, *J. Chem. Phys.*, 1985, **83**, 5338.
57 T. Merle-Méjean, P. Barberis, S. B. Othmane, F. Nardou and P. E. Quintard, *J. Eur. Ceram. Soc.*, 1998, **18**, 1579.
58 P. W. Peacock and J. Robertson, *Appl. Phys. Lett.*, 2003, **83**, 2025.
59 K. Hermansson, G. Gajewski and P. D. Mitev, *J. Phys. Chem. A*, 2008, **112**, 13487.
60 T. Ichikawa, H. Tachikawa, J. Kumagai, T. Kumada and T. Miyazaki, *J. Phys. Chem. A*, 1997, **101**, 7315.
61 A. Eichler, *Phys. Rev. B: Condens. Matter Mater. Phys.*, 2001, **64**, 174103.
62 G. Mahan, *Solid State Ionics*, 1980, **1**, 29.
63 K. Momma and F. Izumi, *J. Appl. Crystallogr.*, 2011, **44**, 1272.